Local Markers for Crystalline Topology

Alexander Cerjan,[1,*] Terry A. Loring,[2] and Hermann Schulz-Baldes[3]
[1]Center for Integrated Nanotechnologies, Sandia National Laboratories, Albuquerque, New Mexico 87185, USA
[2]Department of Mathematics and Statistics, University of New Mexico, Albuquerque, New Mexico 87131, USA
[3]FAU Erlangen-Nürnberg, Department Mathematik, Cauerstr. 11, D-91058 Erlangen, Germany

(Received 2 October 2023; accepted 19 January 2024; published 16 February 2024)

Over the last few years, crystalline topology has been used in photonic crystals to realize edge- and corner-localized states that enhance light-matter interactions for potential device applications. However, the band-theoretic approaches currently used to classify bulk topological crystalline phases cannot predict the existence, localization, or spectral isolation of any resulting boundary-localized modes. While interfaces between materials in different crystalline phases must have topological states at some energy, these states need not appear within the band gap, and thus may not be useful for applications. Here, we derive a class of local markers for identifying material topology due to crystalline symmetries, as well as a corresponding measure of topological protection. As our real-space-based approach is inherently local, it immediately reveals the existence and robustness of topological boundary-localized states, yielding a predictive framework for designing topological crystalline heterostructures. Beyond enabling the optimization of device geometries, we anticipate that our framework will also provide a route forward to deriving local markers for other classes of topology that are reliant upon spatial symmetries.

DOI: 10.1103/PhysRevLett.132.073803

The discovery of crystalline-symmetry protected topological phases, such as obstructed atomic limits [1], fragile topology [2–5], and higher-order topology [6–9], has played a prominent role in the development of artificial topological materials. Indeed, one of the primary features of such materials is that their geometry can be carefully tailored during fabrication, allowing for exquisite control over a system's spatial symmetries [10–12]. In photonic crystals, the edge- and corner-localized modes that can appear at the interfaces between structures in different topological crystalline phases have been used to realize a wide variety of useful phenomena, such as lasers [13–18], single photon routing [19–23], and structures for enhancing harmonic generation [24–27]. Crystalline topology can also be observed in acoustic systems [28–37], where it can protect Fano resonances [38] and enable robust analog signal processing [39].

However, the existing theoretical framework for identifying crystalline topology poses a substantial challenge for the design of many types of artificial materials seeking to leverage these phases' boundary-localized phenomena. At present, this classification framework is rooted in band theory, and diagnoses a system's topology through the calculation of elementary band representations [1,4,40] and symmetry indicators [41–49], or Wilson loops over a system's Brillouin zone [50–52]. Yet, the interface between gapped materials that are in different crystalline-symmetry protected topological phases is not guaranteed to exhibit a localized state at the center of their common band gap, or even within this gap at all [53]. Instead, after designing such a topological heterostructure, the existence, localization, and spectral isolation of any boundary states must be confirmed through additional analysis, such as large-volume simulations of the interface. Although it is possible to combine crystalline symmetries with chiral or particle-hole symmetry to protect the boundary-localized states' frequencies to be at midgap [53,54], many artificial materials, including photonic crystals, cannot realize these additional symmetries. Thus, the most salient properties of many artificial crystalline topological materials for enhancing interactions cannot, in general, be predicted or protected by known band-theoretic approaches.

Here, we introduce a class of local markers for identifying the topology of materials due to their crystalline symmetries. These markers are applicable to both first-order and higher-order topology, and changes in them directly reveal a system's topological boundary-localized states. Moreover, associated with every such marker is a local measure of topological protection, providing a quantitative assessment for the robustness of each boundary-localized state. We show how this framework can be applied to realistic photonic crystals to identify topological corner-localized states that are nearly degenerate with surrounding edge modes. Furthermore, by calculating the local measure of protection for disordered versions of this system, we demonstrate that a topological state's robustness can be independent of its spectral separation from the bulk bands, in contrast to the standard assumption that such a state's robustness is determined by this spectral separation. Looking forward, our framework may both enable the

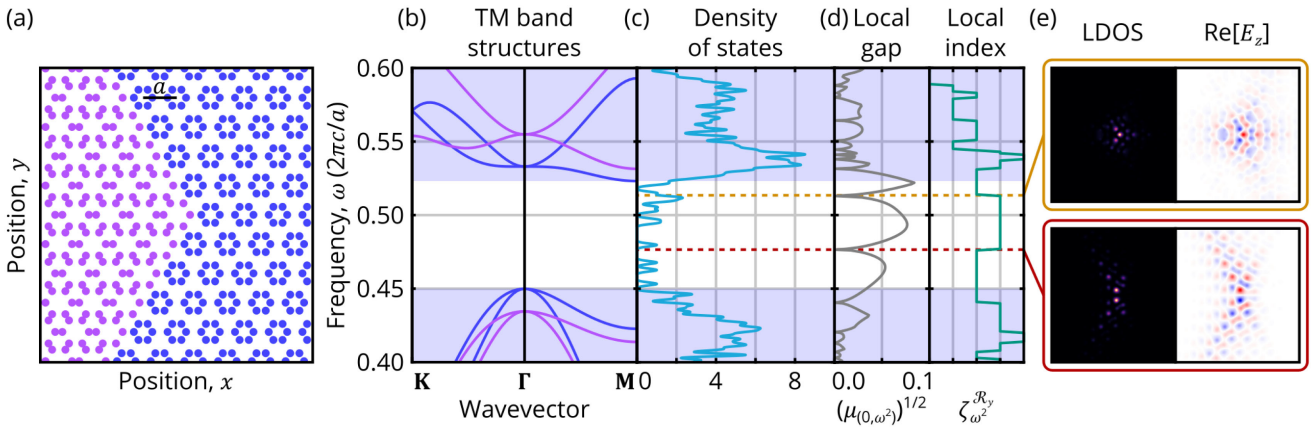

FIG. 1. (a) Diagram of a 2D photonic structure with a 120° corner between crystals formed from expanded (purple) and contracted (blue) hexagonal clusters, bounded by a perfect electric conductor. The high dielectric rods $\varepsilon = 11.7$ embedded in air have radius $r = a/9$ and are offset from being a honeycomb lattice by $\pm 0.06a$, where a is the lattice constant. (b) Bulk TM band structure for the expanded (purple) and contracted (blue) photonic crystals. (c) Density of states for the finite system in (a). (d) Local gap $(\mu_{(0,\omega^2)})^{1/2}$ in units of $2\pi c/a$ and local index $\zeta^{\mathcal{R}_y}_{\omega^2}$ calculated using $\kappa = 0.01(2\pi c)^2/a^3$. Note, $(\mu_{(0,\omega^2)})^{1/2}$ has units of frequency, enabling direct comparison against the system's band structure. In (b)–(d) the shaded regions demarcate those frequencies where bulk states exist. (e) Local density of states (LDOS) at the frequency of the local gap closing and real part of the E_z field for the nearest mode of the system. Orange corresponds to $\omega = 0.515(2\pi c/a)$, and red to $\omega = 0.480(2\pi c/a)$.

prediction of devices predicated on this class of topology while inherently accounting for finite system size effects, and yield insights for deriving local markers for other classes of topology that are reliant upon spatial symmetries, such as those found in moiré systems.

To provide a specific system that exemplifies the difficulties faced in developing artificial topological heterostructures based on crystalline symmetries, we consider a 2D photonic structure consisting of a triangular lattice whose unit cells are decorated with expanded or contracted hexagons of high-dielectric rods [55] that are arranged to form an interface with a 120° corner between the two decoration choices [Fig. 1(a)]. The transverse magnetic (TM) modes of these two different decoration choices have been previously shown to be in different topological crystalline phases [24,27,55–57], and can exhibit topological corner-localized states within their common band gap (Fig. 1). However, as photonic crystals do not generally possess chiral or particle-hole symmetry, these corner-localized states do not appear at the center of the shared gap (without fine-tuning). Thus, even if the topological distinction between the two domains is protected by the bulk band gap, this gap does not protect the localization of the corner states, which could become degenerate with the bulk bands for weaker perturbation strengths than are necessary for a bulk topological phase transition (usually resulting in the delocalization of the corner states [58–60]).

A framework designed to identify the topological interface-localized states stemming from the system's crystalline symmetries requires two components: an invariant that distinguishes topological phases, and an argument showing that shifts in the invariant guarantee the appearance of boundary-localized states. Here, we build such a framework by starting with the spectral localizer [61–68], which is known to be connected to topology arising from local discrete symmetries (i.e., the Altland-Zirnbauer classes [69–71]). The spectral localizer is a composite operator that combines the eigenvalue problems of a finite system's Hamiltonian $(H - E\mathbf{1})\boldsymbol{\phi} = 0$ and position operators $(X - x\mathbf{1})\boldsymbol{\phi} = 0$ using a Clifford representation. For a system with a single relevant position operator, the spectral localizer can be written as

$$\begin{aligned} L_{(x,E)}(X,H) &= (H - E\mathbf{1}) \otimes \sigma_x + \kappa(X - x\mathbf{1}) \otimes \sigma_y \\ &= \begin{pmatrix} 0 & (H - E\mathbf{1}) - i\kappa(X - x\mathbf{1}) \\ (H - E\mathbf{1}) + i\kappa(X - x\mathbf{1}) & 0 \end{pmatrix}, \end{aligned} \tag{1}$$

where the Pauli matrices σ_x and σ_y are used as the Clifford representation. Here, $\kappa > 0$ is a tuning coefficient to ensure consistent units and comparable contributions of all summands, and $\mathbf{1}$ is the identity. The approximate scale of κ is set by the bulk band gap g and the length of the finite system l in the relevant dimension, $\kappa \approx 2g/l$, see Supplemental Material Sec. SIII [72]. In cases where the matrix arguments are implied by their context, they will be omitted, e.g., $L_{(x,E)} = L_{(x,E)}(X,H)$.

Unlike standard eigenvalue equations, where the eigenvalues are determined by their respective operators, the position x and energy E are inputs in the spectral localizer, and its spectrum quantifies whether the system exhibits a state approximately localized at (x, E) [83], or how large of a system perturbation δH is needed to obtain such a state. In particular, if the minimum distance over all of the eigenvalues of $L_{(x,E)}$ to 0,

$$\mu_{(x,E)}(X, H) = \min(|\mathrm{spec}[L_{(x,E)}(X, H)]|), \tag{2}$$

is small relative to $\|[H, \kappa X]\|$, such an approximately localized state exists [83]. Here, $\mathrm{spec}[L]$ denotes the spectrum of L. Conversely, if $\mu_{(x,E)}$ is large, a perturbation with norm $\|\delta H\| \gtrapprox \mu_{(x,E)}(X, H)$ is required for such a state to be found, i.e., for $\mu_{(x,E)}(X, H + \delta H) = 0$. As such, $\mu_{(x,E)}$ can be heuristically understood as a "local band gap."

As crystalline symmetries are independent of a system's local discrete symmetries, a crystalline invariant should be applicable to any system regardless of the presence or absence of such discrete symmetries. Thus, a local crystalline topological marker should be given by the signature of an invertible Hermitian matrix, i.e., its number of positive eigenvalues minus its number of negative ones. This is analogous to how, for example, the 0th Chern number of a 0D system is given by the partitioning of its Hamiltonian's eigenvalues about a chosen band gap; the relevant invertible Hermitian matrix here is $H - E_g\mathbf{1}$, where E_g is the band gap's central energy [84]. (In contrast, topology originating from phenomena like parity switches are not related to a matrix's signature, but can only manifest in the presence of specific local discrete symmetries.) However, even though $L_{(x,E)}$ is Hermitian, its block off-diagonal structure guarantees that its eigenvalues are always symmetric about 0 for any choice of x and E.

Instead, we seek to remove the duplication in $\mathrm{spec}[L_{(x,E)}]$ using the system's crystalline symmetry, and then define an invariant based on this reduced spectrum. In particular, a local crystalline topological marker can be constructed from $L_{(x,E)}$ if the system has a unitary crystalline symmetry $\mathcal{S}$ that satisfies $\mathcal{S}^2 = \mathbf{1}$, $H\mathcal{S} = \mathcal{S}H$, and $X\mathcal{S} = -\mathcal{S}X$. Multiplying the off-diagonal blocks in Eq. (1) by $\mathcal{S}$ at $x = 0$ yields the *symmetry-reduced spectral localizer*

$$\tilde{L}_E^{\mathcal{S}}(X, H) = (H - E\mathbf{1} + i\kappa X)\mathcal{S}, \tag{3}$$

(A related operator can be constructed for 1D chiral symmetric systems [60,85].) Remarkably, $\tilde{L}_E^{\mathcal{S}} = (\tilde{L}_E^{\mathcal{S}})^\dagger$ is Hermitian due to the above symmetry relations. Even though $\tilde{L}_E^{\mathcal{S}}$ is only built from a single block of $L_{(0,E)}$, it contains all of the essential spectral information in $L_{(0,E)}$, as

$$\lambda \in \mathrm{spec}[\tilde{L}_E^{\mathcal{S}}(X, H)] \Rightarrow \pm\lambda \in \mathrm{spec}[L_{(0,E)}(X, H)]; \tag{4}$$

see Supplemental Material Sec. SI [72]. Hence, $\tilde{L}_E^{\mathcal{S}}$ has only "half of the eigenvalues" of $L_{(0,E)}$, and these eigenvalues need not lie symmetrically around 0. Thus, a local crystalline topological marker can be constructed as

$$\zeta_E^{\mathcal{S}}(X, H) = \frac{1}{2}\mathrm{sig}[\tilde{L}_E^{\mathcal{S}}(X, H)], \tag{5}$$

where $\mathrm{sig}[\tilde{L}_E^{\mathcal{S}}]$ is the matrix's signature. For a system with an even or odd number of states, $\zeta_E^{\mathcal{S}}$ is integer or half-integer, but the changes in $\zeta_E^{\mathcal{S}}$ are always integer valued (and define the spectral flow, which provides a rigorous generalization to the thermodynamic limit, see Supplemental Material Sec. SI [72]). Note that $\zeta_E^{\mathcal{S}}$ is only defined when $\tilde{L}_E^{\mathcal{S}}$ possesses a spectral gap about 0, that is, $\mu_{(0,E)} \neq 0$. Moreover, one can prove that pairs (X, H) describing finite systems with the same $\zeta_E^{\mathcal{S}}$ can be path connected to each other while preserving $\mathcal{S}$ and maintaining $\mu_{(0,E)} > 0$, while this is impossible for systems with different $\zeta_E^{\mathcal{S}}$, see Supplemental Material Sec. SII [72].

The local marker $\zeta_E^{\mathcal{S}}$ is an indicator for topological boundary states. Specifically, $\zeta_E^{\mathcal{S}}$ can only change its value at some energy E_c if $0 \in \mathrm{spec}[\tilde{L}_{E_c}^{\mathcal{S}}]$ so that one of the eigenvalues can switch its sign. But, due to Eq. (4), this requires that $\mu_{(0,E_c)} = 0$. In turn, a vanishing local gap guarantees the existence of an eigenvalue of H near E_c, whose corresponding eigenstate is centered at $x = 0$ [72,83]. If the local gap closing occurs within a bulk band gap, it must correspond to a boundary-localized state. Furthermore, $\mu_{(0,E)} \neq 0$ provides a measure of topological protection, as a perturbation must close the local gap for the topology to change. Thus, altogether, $\zeta_E^{\mathcal{S}}$ both distinguishes crystalline topological phases with respect to $\mathcal{S}$ and changes in its value guarantee that the system possesses a topological state.

To demonstrate that $\zeta_E^{\mathcal{S}}$ is a useful invariant for predicting the behavior of artificial topological materials, we apply the spectral localizer framework to the heterostructure considered in Fig. 1(a). We start with the second-order differential equation form of Maxwell's time-harmonic equations for TM modes

$$\nabla^2 E_z(\mathbf{x}) = -\omega^2 \varepsilon(\mathbf{x}) E_z(\mathbf{x}), \tag{6}$$

in which $E_z(\mathbf{x})$ is the z component of the electromagnetic field, ω is the frequency, $\varepsilon(\mathbf{x}) > 0$ is the spatially dependent dielectric distribution, and the magnetic permeability is assumed to be the identity. Using standard finite-difference methods to approximate the Laplacian, we obtain the pair of finite matrices $\nabla^2 \to W$ and M, such that M can be diagonal with $[M]_{j,j} = \varepsilon(\mathbf{x}_j)$, where $\mathbf{x}_j = (x_j, y_j)$ is the jth vertex in the discretization. Thus, Eq. (6) can be written as the Hermitian eigenvalue problem

$$(-M^{-1/2}WM^{-1/2} - \omega^2\mathbf{1})\boldsymbol{\psi} = 0, \tag{7}$$

where $\boldsymbol{\psi} = M^{1/2}E_z$. Note that if $[M, \mathcal{S}] = 0$, then $[M^{-1/2}, \mathcal{S}] = 0$. The discretization of the system also defines its position operators, which can also be chosen to be diagonal; for the 2D system considered in Fig. 1, $[X]_{j,j} = x_j$ and $[Y]_{j,j} = y_j$. Overall, this formulation of Maxwell's equations and the subsequent choice of discretization are chosen to preserve a dielectric distribution's crystalline symmetries.

The heterostructure with a 120° corner in its interface that is considered in Fig. 1 possesses a reflection symmetry $\mathcal{R}_y$ about the $y = 0$ axis. Thus, as $H\mathcal{R}_y = \mathcal{R}_y H$, $Y\mathcal{R}_y = -\mathcal{R}_y Y$, and $\mathcal{R}_y^2 = \mathbf{1}$, this symmetry can be used to define a $\mathcal{R}_y$-symmetrized spectral localizer and associated local marker as

$$\tilde{L}_{\omega^2}^{\mathcal{R}_y} = (H - \omega^2\mathbf{1} + i\kappa Y)\mathcal{R}_y, \qquad \zeta_{\omega^2}^{\mathcal{R}_y} = \frac{1}{2}\mathrm{sig}\left[\tilde{L}_{\omega^2}^{\mathcal{R}_y}\right], \tag{8}$$

where $H = -M^{-1/2}WM^{-1/2}$, and the local gap at $y = 0$ is given by $\mu_{(0,\omega^2)} = \min(|\mathrm{spec}[\tilde{L}_{\omega^2}^{\mathcal{R}_y}]|)$. Although the system in Fig. 1(a) is 2D, $\tilde{L}_{\omega^2}^{\mathcal{R}_y}$ and the associated local index and gap only use one of its two position operators (similar to real-space formulations of other weak invariants [66,67]). This effectively forces $\zeta_{\omega^2}^{\mathcal{R}_y}$ and $\mu_{(0,\omega^2)}$ to focus on the system's reflection center.

As can be seen in Figs. 1(d) and 1(e), the corner heterostructure exhibits two topological corner-localized states within its bulk band gap. Although these states are difficult to uniquely identify in the system's density of states (DOS) due to the surrounding, nearly degenerate edge-localized modes [Figs. 1(c) and S2], the corner states can be immediately identified using the system's local gap, as they are energetically close to the local gap closing within the heterostructure's bulk band gap and do not come in reflection symmetric pairs (see Supplemental Material Sec. SVII [72]). Moreover, at both of these closings the local topological index changes, proving that both corner states are topological with respect to $\mathcal{R}_y$. Finally, the large local gaps on either side of these corner states indicate that they are both robust against fabrication imperfections. Quantitatively similar results appear for a range of κ, see Supplemental Material Sec. SIII [72]. Note that although there are many local index changes within the spectral extent of the bulk bands, the tiny local gaps within these regions indicate that these topological phases have vanishing protection.

In contrast to the assumption that crystalline topological states closer to the center of the common bulk band gap are better protected against disorder, the local gap [Fig. 1(d)] reveals that the higher-frequency corner-localized state in this system has more topological protection than the lower-frequency corner state despite being closer in frequency to the bulk bands. In general, a perturbation δH with strength $\|\delta H\| \gtrapprox \mu_{(0,\omega^2)}$ is necessary to change the system's local topology, but this criterion is not sufficient for photonic systems—an arbitrary $H + \delta H$ cannot generally be decomposed into a physically meaningful combination of a local permittivity and Laplacian, per Eq. (7). Instead, the increased protection of the higher-frequency state can be seen by finding the dielectric defect strength necessary to annihilate each of the corner states. In Fig. 2 we consider two different perturbations that respect $\mathcal{R}_y$, each tailored to affect one corner mode by changing the permittivity of the rod(s) the state has its maximum support on [Fig. 1(e)]. For the lower-frequency corner state's perturbation [Figs. 2(a) and 2(c)], a change in the permittivity of $\delta\varepsilon = 1.17$ is needed to annihilate the topological state by combining it with a state from the lower-frequency bulk bands. In comparison, the necessary perturbation to annihilate the higher-frequency corner state is $\delta\varepsilon = -4.28$ [Figs. 2(b) and 2(d)], despite a similar overlap of the corner-localized state and the perturbation (see Supplemental Material Sec. SIV [72]). These results provide evidence that the local gap yields an experimentally relevant hierarchy of protection for a photonic system's topological states.

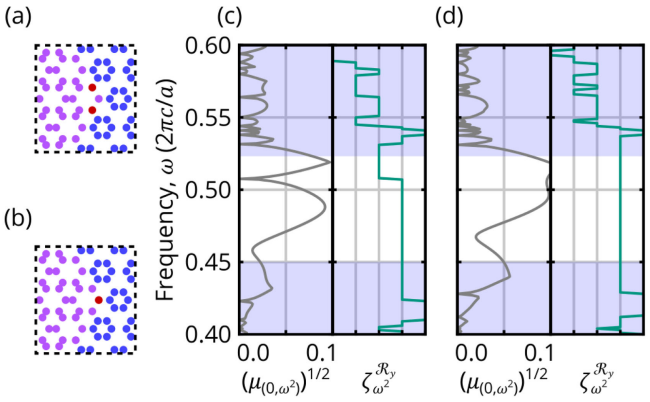

FIG. 2. (a),(b) Zoomed in diagram of the perturbed rods (red) in the photonic crystal corner heterostructure from Fig. 1(a) tailored to the lower-frequency (a) and higher-frequency (b) corner states. (c) Local gap $(\mu_{(0,\omega^2)})^{(1/2)}$ in units of $2\pi c/a$ and local index $\zeta_{\omega^2}^{\mathcal{R}_y}$ calculated using $\kappa = 0.01(2\pi c)^2/a^3$ for the lower-frequency perturbation with $\delta\varepsilon = \varepsilon_{\mathrm{red}} - \varepsilon = 1.17$. (d) Similar to (c), except using the higher-frequency perturbation with $\delta\varepsilon = -4.28$. The shaded regions in (c),(d) demarcate those frequencies within the bulk bands.

The local crystalline topological marker $\zeta_E^{\mathcal{S}}$ is also applicable to first-order topology. Section SV in the Supplemental Material provides an example of classifying edge states using this framework [72].

Having proved that $\zeta_E^{\mathcal{S}}$ is a useful local marker indicating the existence of topological boundary states and that $\mu_{(0,E)}$ is its associated measure of protection, we now provide a physical interpretation for changes in its value. Consider the eigenvalue l_E of $\tilde{L}_E^{\mathcal{S}}$ closest to zero and its

corresponding eigenvector $\boldsymbol{\phi}_E$, and note the square of the symmetry-reduced spectral localizer,

$$(\tilde{L}_E^{\mathcal{S}})^2 = (H - E\mathbf{1})^2 - i\kappa[H, X] + \kappa^2 X^2. \tag{9}$$

For systems with only local couplings, $\|[H, X]\|$ is proportional to the lattice constant times the system's energy scale, and as such is of order 1 in the system's natural units. Thus, as generally κ is small (which guarantees the robustness of the spectral localizer to different choices of κ [63]), to leading order one finds that

$$l_E^2 \boldsymbol{\phi}_E \approx (H - E\mathbf{1})^2 \boldsymbol{\phi}_E. \tag{10}$$

Now, let E_c be an energy where the local gap closes $\mu_{(0,E_c)} = 0$, such that $l_{E_c} = 0$. If the spectrum of H is non-degenerate (possibly through the addition of a small amount of symmetry-preserving disorder), one finds $\boldsymbol{\phi}_{E_c} \approx \boldsymbol{\psi}_b$ and $E_c \approx E_b$, where $H\boldsymbol{\psi}_b = E_b\boldsymbol{\psi}_b$. Thus, in the vicinity of the local gap closing where there is only a single relevant eigenstate of the Hamiltonian, one finds that

$$l_E \approx s_b((E_b - E) + i\kappa \boldsymbol{\psi}_b^\dagger X \boldsymbol{\psi}_b), \tag{11}$$

where $\mathcal{S}\boldsymbol{\psi}_b = s_b\boldsymbol{\psi}_b$ with $s_b = \pm 1$. But, as X anti-commutes with $\mathcal{S}$, $\boldsymbol{\psi}_b^\dagger X \boldsymbol{\psi}_b = 0$. Altogether, for $E \approx E_c$,

$$l_E \approx -s_b(E - E_c), \tag{12}$$

i.e., the eigenvalue of $\tilde{L}_E^{\mathcal{S}}$ closest to zero is linear near a local gap closing, and the change ± 1 of $\zeta_E^{\mathcal{S}}$ across E_c is opposite to the symmetry eigenvalue of the Hamiltonian's corresponding topological state. [See Supplemental Material Sec. SI [72] for a more detailed derivation of Eq. (12).] The prediction of Eq. (12) is realized in the system from Fig. 1; simulations show that for the corner-localized state near $\omega = 0.480(2\pi c/a)$, the index $\zeta_{\omega^2}^{\mathcal{R}_y}$ increases by $+1$ (for increasing ω) when the local gap closes, and the corresponding eigenstate of the system is odd ($s_b = -1$) with respect to $\mathcal{R}_y$. The opposite behavior is observed for the corner-localized state near $\omega = 0.515(2\pi c/a)$, with $\zeta_{\omega^2}^{\mathcal{R}_y}$ decreasing as the corner-localized eigenstate is even with respect to $\mathcal{R}_y$. Thus, $\zeta_E^{\mathcal{S}}$ is identifying atomic limits with different numbers of states that are either even or odd with respect to $\mathcal{S}$.

In conclusion, we have introduced a class of local crystalline topological markers $\zeta_E^{\mathcal{S}}$ and their associated measure of topological protection rooted in the spectral localizer. Unlike traditional theories of crystalline topology that only yield $\mathbb{Z}_N$ invariants [43,53,86–88], the local markers derived here are $\mathbb{Z}$ invariants that can identify multiple topological states per band gap beyond those predicted by a system's fractional filling anomaly (see Supplemental Material Sec. SVIII [72]). Thus, further work is required to connect these two frameworks by accounting for the different phenomena each is sensitive to. More immediately, our operator-based framework should be useful for the design of materials seeking to leverage crystalline topology to enhance interactions by optimizing over the predicted measure of a state's topological robustness. Furthermore, by providing a physically motivated derivation of our local markers, our work may aid future theoretical studies in finding local markers for other classes of topology, and in particular the topology seen in moiré systems.

A. C. and T. L. acknowledge support from the Laboratory Directed Research and Development program at Sandia National Laboratories. H. S.-B. acknowledges support from DFG under Grant No. SCHU 1358/8-1. T. L. acknowledges support from the National Science Foundation, Grant No. DMS-2110398. A. C. acknowledges support from the U.S. Department of Energy, Office of Basic Energy Sciences, Division of Materials Sciences and Engineering. This work was performed, in part, at the Center for Integrated Nanotechnologies, an Office of Science User Facility operated for the U.S. Department of Energy (DOE) Office of Science. Sandia National Laboratories is a multimission laboratory managed and operated by National Technology & Engineering Solutions of Sandia, LLC, a wholly owned subsidiary of Honeywell International, Inc., for the U.S. DOE's National Nuclear Security Administration under Contract No. DE-NA-0003525. The views expressed in the Letter do not necessarily represent the views of the U.S. DOE or the United States Government.

*awcerja@sandia.gov

[1] Barry Bradlyn, L. Elcoro, Jennifer Cano, M. G. Vergniory, Zhijun Wang, C. Felser, M. I. Aroyo, and B. Andrei Bernevig, Topological quantum chemistry, Nature (London) **547**, 298 (2017).
[2] Hoi Chun Po, Haruki Watanabe, and Ashvin Vishwanath, Fragile topology and Wannier obstructions, Phys. Rev. Lett. **121**, 126402 (2018).
[3] Z. Wang, B. J. Wieder, J. Li, B. Yan, and B. A. Bernevig, Higher-order topology, monopole nodal lines, and the origin of large Fermi arcs in transition metal dichalcogenides $x\text{te}_2$ (x = Mo, W), Phys. Rev. Lett. **123**, 186401 (2019).
[4] M. B. de Paz, M. G. Vergniory, D. Bercioux, A. García-Etxarri, and B. Bradlyn, Engineering fragile topology in photonic crystals: Topological quantum chemistry of light, Phys. Rev. Res. **1**, 032005(R) (2019).
[5] Zhi-Da Song, Luis Elcoro, and B. Andrei Bernevig, Twisted bulk-boundary correspondence of fragile topology, Science **367**, 794 (2020).
[6] Wladimir A. Benalcazar, B. Andrei Bernevig, and Taylor L. Hughes, Quantized electric multipole insulators, Science **357**, 61 (2017).

[7] W. A. Benalcazar, B. A. Bernevig, and T. L. Hughes, Electric multipole moments, topological multipole moment pumping, and chiral hinge states in crystalline insulators, Phys. Rev. B **96**, 245115 (2017).
[8] Zhida Song, Zhong Fang, and Chen Fang, $(d-2)$-dimensional edge states of rotation symmetry protected topological states, Phys. Rev. Lett. **119**, 246402 (2017).
[9] Biye Xie, Hai-Xiao Wang, Xiujuan Zhang, Peng Zhan, Jian-Hua Jiang, Minghui Lu, and Yanfeng Chen, Higher-order band topology, Nat. Rev. Phys. **3**, 520 (2021).
[10] Julian Schulz, Sachin Vaidya, and Christina Jörg, Topological photonics in 3D micro-printed systems, APL Photonics **6**, 080901 (2021).
[11] Martin Maldovan, Sound and heat revolutions in phononics, Nature (London) **503**, 209 (2013).
[12] Haoran Xue, Yihao Yang, and Baile Zhang, Topological acoustics, Nat. Rev. Mater. **7**, 974 (2022).
[13] Yongquan Zeng, Udvas Chattopadhyay, Bofeng Zhu, Bo Qiang, Jinghao Li, Yuhao Jin, Lianhe Li, Alexander Giles Davies, Edmund Harold Linfield, Baile Zhang, Yidong Chong, and Qi Jie Wang, Electrically pumped topological laser with valley edge modes, Nature (London) **578**, 246 (2020).
[14] Zhen-Qian Yang, Zeng-Kai Shao, Hua-Zhou Chen, Xin-Rui Mao, and Ren-Min Ma, Spin-momentum-locked edge mode for topological vortex lasing, Phys. Rev. Lett. **125**, 013903 (2020).
[15] Zeng-Kai Shao, Hua-Zhou Chen, Suo Wang, Xin-Rui Mao, Zhen-Qian Yang, Shao-Lei Wang, Xing-Xiang Wang, Xiao Hu, and Ren-Min Ma, A high-performance topological bulk laser based on band-inversion-induced reflection, Nat. Nanotechnol. **15**, 67 (2020).
[16] Ha-Reem Kim, Min-Soo Hwang, Daria Smirnova, Kwang-Yong Jeong, Yuri Kivshar, and Hong-Gyu Park, Multipolar lasing modes from topological corner states, Nat. Commun. **11**, 5758 (2020).
[17] Yongkang Gong, Stephan Wong, Anthony J. Bennett, Diana L. Huffaker, and Sang Soon Oh, topological insulator laser using valley-Hall photonic crystals, ACS Photonics **7**, 2089 (2020).
[18] Alex Dikopoltsev, Tristan H. Harder, Eran Lustig, Oleg A. Egorov, Johannes Beierlein, Adriana Wolf, Yaakov Lumer, Monika Emmerling, Christian Schneider, Sven Höfling, Mordechai Segev, and Sebastian Klembt, Topological insulator vertical-cavity laser array, Science **373**, 1514 (2021).
[19] Sabyasachi Barik, Aziz Karasahin, Christopher Flower, Tao Cai, Hirokazu Miyake, Wade DeGottardi, Mohammad Hafezi, and Edo Waks, A topological quantum optics interface, Science **359**, 666 (2018).
[20] Sabyasachi Barik, Aziz Karasahin, Sunil Mittal, Edo Waks, and Mohammad Hafezi, Chiral quantum optics using a topological resonator, Phys. Rev. B **101**, 205303 (2020).
[21] Nikhil Parappurath, Filippo Alpeggiani, L. Kuipers, and Ewold Verhagen, Direct observation of topological edge states in silicon photonic crystals: Spin, dispersion, and chiral routing, Sci. Adv. **6**, eaaw4137 (2020).
[22] Sonakshi Arora, Thomas Bauer, René Barczyk, Ewold Verhagen, and L. Kuipers, Direct quantification of topological protection in symmetry-protected photonic edge states at telecom wavelengths, Light. Light. **10**, 9 (2021).
[23] Nils Valentin Hauff, Hanna Le Jeannic, Peter Lodahl, Stephen Hughes, and Nir Rotenberg, Chiral quantum optics in broken-symmetry and topological photonic crystal waveguides, Phys. Rev. Res. **4**, 023082 (2022).
[24] D. Smirnova, S. Kruk, D. Leykam, E. Melik-Gaykazyan, D.-Y. Choi, and Y. Kivshar, Third-harmonic generation in photonic topological metasurfaces, Phys. Rev. Lett. **123**, 103901 (2019).
[25] Mikhail I. Shalaev, Wiktor Walasik, Alexander Tsukernik, Yun Xu, and Natalia M. Litchinitser, Robust topologically protected transport in photonic crystals at telecommunication wavelengths, Nat. Nanotechnol. **14**, 31 (2019).
[26] Yasutomo Ota, Feng Liu, Ryota Katsumi, Katsuyuki Watanabe, Katsunori Wakabayashi, Yasuhiko Arakawa, and Satoshi Iwamoto, Photonic crystal nanocavity based on a topological corner state, Optica **6**, 786 (2019).
[27] Sergey S. Kruk, Wenlong Gao, Duk-Yong Choi, Thomas Zentgraf, Shuang Zhang, and Yuri Kivshar, Nonlinear imaging of nanoscale topological corner states, Nano Lett. **21**, 4592 (2021).
[28] Marc Serra-Garcia, Valerio Peri, Roman Süsstrunk, Osama R Bilal, Tom Larsen, Luis Guillermo Villanueva, and Sebastian D Huber, Observation of a phononic quadrupole topological insulator, Nature (London) **555**, 342 (2018).
[29] Xiang Ni, Matthew Weiner, Andrea Alù, and Alexander B. Khanikaev, Observation of higher-order topological acoustic states protected by generalized chiral symmetry, Nat. Mater. **18**, 113 (2019).
[30] Haoran Xue, Yahui Yang, Fei Gao, Yidong Chong, and Baile Zhang, Acoustic higher-order topological insulator on a kagome lattice, Nat. Mater. **18**, 108 (2019).
[31] Haoran Xue, Yahui Yang, Guigeng Liu, Fei Gao, Yidong Chong, and Baile Zhang, Realization of an acoustic third-order topological insulator, Phys. Rev. Lett. **122**, 244301 (2019).
[32] Xiujuan Zhang, Hai-Xiao Wang, Zhi-Kang Lin, Yuan Tian, Biye Xie, Ming-Hui Lu, Yan-Feng Chen, and Jian-Hua Jiang, Second-order topology and multidimensional topological transitions in sonic crystals, Nat. Phys. **15**, 582 (2019).
[33] Xiujuan Zhang, Bi-Ye Xie, Hong-Fei Wang, Xiangyuan Xu, Yuan Tian, Jian-Hua Jiang, Ming-Hui Lu, and Yan-Feng Chen, Dimensional hierarchy of higher-order topology in three-dimensional sonic crystals, Nat. Commun. **10**, 5331 (2019).
[34] Xiang Ni, Mengyao Li, Matthew Weiner, Andrea Alù, and Alexander B. Khanikaev, Demonstration of a quantized acoustic octupole topological insulator, Nat. Commun. **11**, 2108 (2020).
[35] Haoran Xue, Yong Ge, Hong-Xiang Sun, Qiang Wang, Ding Jia, Yi-Jun Guan, Shou-Qi Yuan, Yidong Chong, and Baile Zhang, Observation of an acoustic octupole topological insulator, Nat. Commun. **11**, 2442 (2020).
[36] Xiujuan Zhang, Zhi-Kang Lin, Hai-Xiao Wang, Zhan Xiong, Yuan Tian, Ming-Hui Lu, Yan-Feng Chen, and Jian-Hua Jiang, Symmetry-protected hierarchy of anomalous multipole topological band gaps in nonsymmorphic metacrystals, Nat. Commun. **11**, 65 (2020).
[37] Valerio Peri, Zhi-Da Song, Marc Serra-Garcia, Pascal Engeler, Raquel Queiroz, Xueqin Huang, Weiyin Deng,

Zhengyou Liu, B. Andrei Bernevig, and Sebastian D. Huber, Experimental characterization of fragile topology in an acoustic metamaterial, Science **367**, 797 (2020).
[38] F. Zangeneh-Nejad and R. Fleury, Topological Fano resonances, Phys. Rev. Lett. **122**, 014301 (2019).
[39] Farzad Zangeneh-Nejad and Romain Fleury, Topological analog signal processing, Nat. Commun. **10**, 2058 (2019).
[40] J. Cano, B. Bradlyn, Z. Wang, L. Elcoro, M. G. Vergniory, C. Felser, M. I. Aroyo, and B. A. Bernevig, Building blocks of topological quantum chemistry: Elementary band representations, Phys. Rev. B **97**, 035139 (2018).
[41] Jorrit Kruthoff, Jan de Boer, Jasper van Wezel, Charles L. Kane, and Robert-Jan Slager, Topological classification of crystalline insulators through band structure combinatorics, Phys. Rev. X **7**, 041069 (2017).
[42] Hoi Chun Po, Ashvin Vishwanath, and Haruki Watanabe, Symmetry-based indicators of band topology in the 230 space groups, Nat. Commun. **8**, 50 (2017).
[43] Wladimir A. Benalcazar, Tianhe Li, and Taylor L. Hughes, Quantization of fractional corner charge in C_n-symmetric higher-order topological crystalline insulators, Phys. Rev. B **99**, 245151 (2019).
[44] Haruki Watanabe and Ling Lu, Space group theory of photonic bands, Phys. Rev. Lett. **121**, 263903 (2018).
[45] Ian Mondragon-Shem and Taylor L. Hughes, Robust topological invariants of topological crystalline phases in the presence of impurities, arXiv:1906.11847.
[46] Saavanth Velury, Barry Bradlyn, and Taylor L. Hughes, Topological crystalline phases in a disordered inversion-symmetric chain, Phys. Rev. B **103**, 024205 (2021).
[47] Vaibhav Gupta and Barry Bradlyn, Wannier-function methods for topological modes in one-dimensional photonic crystals, Phys. Rev. A **105**, 053521 (2022).
[48] Thomas Christensen, Hoi Chun Po, John D. Joannopoulos, and Marin Soljačić, Location and topology of the fundamental gap in photonic crystals, Phys. Rev. X **12**, 021066 (2022).
[49] Ali Ghorashi, Sachin Vaidya, Mikael Rechtsman, Wladimir Benalcazar, Marin Soljačić, and Thomas Christensen, Prevalence of two-dimensional photonic topology, arXiv:2307.15701.
[50] J. Zak, Berry's phase for energy bands in solids, Phys. Rev. Lett. **62**, 2747 (1989).
[51] A. Alexandradinata, X. Dai, and B. A. Bernevig, Wilson-loop characterization of inversion-symmetric topological insulators, Phys. Rev. B **89**, 155114 (2014).
[52] Hai-Xiao Wang, Guang-Yu Guo, and Jian-Hua Jiang, Band topology in classical waves: Wilson-loop approach to topological numbers and fragile topology, New J. Phys. **21**, 093029 (2019).
[53] Sachin Vaidya, Ali Ghorashi, Thomas Christensen, Mikael C. Rechtsman, and Wladimir A. Benalcazar, Topological phases of photonic crystals under crystalline symmetries, Phys. Rev. B **108**, 085116 (2023).
[54] Minwoo Jung, Yang Yu, and Gennady Shvets, Exact higher-order bulk-boundary correspondence of corner-localized states, Phys. Rev. B **104**, 195437 (2021).
[55] Long-Hua Wu and Xiao Hu, Scheme for achieving a topological photonic crystal by using dielectric material, Phys. Rev. Lett. **114**, 223901 (2015).
[56] Simon Yves, Romain Fleury, Thomas Berthelot, Mathias Fink, Fabrice Lemoult, and Geoffroy Lerosey, Crystalline metamaterials for topological properties at subwavelength scales, Nat. Commun. **8**, 16023 (2017).
[57] Maxim A. Gorlach, Xiang Ni, Daria A. Smirnova, Dmitry Korobkin, Dmitry Zhirihin, Alexey P. Slobozhanyuk, Pavel A. Belov, Andrea Alù, and Alexander B. Khanikaev, Far-field probing of leaky topological states in all-dielectric metasurfaces, Nat. Commun. **9**, 909 (2018).
[58] Wladimir A. Benalcazar and Alexander Cerjan, Bound states in the continuum of higher-order topological insulators, Phys. Rev. B **101**, 161116(R) (2020).
[59] Alexander Cerjan, Marius Jürgensen, Wladimir A. Benalcazar, Sebabrata Mukherjee, and Mikael C. Rechtsman, Observation of a higher-order topological bound state in the continuum, Phys. Rev. Lett. **125**, 213901 (2020).
[60] Alexander Cerjan and Terry A. Loring, Local invariants identify topology in metals and gapless systems, Phys. Rev. B **106**, 064109 (2022).
[61] Terry A Loring, K-theory and pseudospectra for topological insulators, Ann. Phys. (Amsterdam) **356**, 383 (2015).
[62] I. C. Fulga, D. I. Pikulin, and T. A. Loring, Aperiodic weak topological superconductors, Phys. Rev. Lett. **116**, 257002 (2016).
[63] Terry A. Loring and Hermann Schulz-Baldes, Finite volume calculation of K-theory invariants, New York J. Math. **23**, 1111 (2017), http://nyjm.albany.edu/j/2017/23-48.html.
[64] Terry A. Loring and Hermann Schulz-Baldes, The spectral localizer for even index pairings, J. Noncommut. Geom. **14**, 1 (2020).
[65] Nora Doll and Hermann Schulz-Baldes, Skew localizer and $\mathbb{Z}_2$-flows for real index pairings, Adv. Math. **392**, 108038 (2021).
[66] Hermann Schulz-Baldes and Tom Stoiber, The spectral localizer for semifinite spectral triples, Proc. Am. Math. Soc. **149**, 121 (2021).
[67] Hermann Schulz-Baldes and Tom Stoiber, Invariants of disordered semimetals via the spectral localizer, Europhys. Lett. **136**, 27001 (2022).
[68] Hermann Schulz-Baldes and Tom Stoiber, Spectral localization for semimetals and Callias operators, J. Math. Phys. (N.Y.) **64**, 081901 (2023).
[69] Andreas P. Schnyder, Shinsei Ryu, Akira Furusaki, and Andreas W. W. Ludwig, Classification of topological insulators and superconductors in three spatial dimensions, Phys. Rev. B **78**, 195125 (2008).
[70] Alexei Kitaev, Periodic table for topological insulators and superconductors, AIP Conf. Proc. **1134**, 22 (2009).
[71] Shinsei Ryu, Andreas P. Schnyder, Akira Furusaki, and Andreas W. W. Ludwig, Topological insulators and superconductors: Tenfold way and dimensional hierarchy, New J. Phys. **12**, 065010 (2010).
[72] See Supplemental Material at http://link.aps.org/supplemental/10.1103/PhysRevLett.132.073803 for a discussion of the connection between the spectrum and singular values of the spectral localizer and manipulations off-diagonal blocks, as well as a proof of how systems with the same symmetry and local marker can be path continued to one another while preserving the symmetry and without

closing the local gap. The Supplemental Material contains Refs. [73–82].

[73] Nora Doll, Hermann Schulz-Baldes, and Nils Waterstraat, *Spectral Flow: A Functional Analytic and Index-Theoretic Approach* (Walter de Gruyter GmbH & Co KG, Berlin/Boston, 2023), Vol. 94.

[74] Tosio Kato, *Perturbation Theory for Linear Operators* (Springer Science & Business Media, New York, 2013), Vol. 132.

[75] Huaxin Lin, Almost commuting selfadjoint matrices and applications, in *Operator Algebras and their Applications (Waterloo, ON, 1994/1995)*, Fields Inst. Commun. Vol. 13 (American Mathematical Society, Providence, RI, 1997), pp. 193–233.

[76] M. B. Hastings, Topology and phases in fermionic systems, J. Stat. Mech. 01 (2008) L01001.

[77] Terry A Loring and Adam PW Sørensen, Almost commuting unitary matrices related to time reversal, Commun. Math. Phys. **323**, 859 (2013).

[78] Terry A Loring and Adam PW Sørensen, Almost commuting self-adjoint matrices: The real and self-dual cases, Rev. Math. Phys. **28**, 1650017 (2016).

[79] Kahlil Y. Dixon, Terry A. Loring, and Alexander Cerjan, Classifying topology in photonic heterostructures with gapless environments, Phys. Rev. Lett. **131**, 213801 (2023).

[80] Nora Doll and Hermann Schulz-Baldes, Approximate symmetries and conservation laws in topological insulators and associated $\mathbb{Z}$-invariants, Ann. Phys. (Amsterdam) **419**, 168238 (2020).

[81] Alexander Cerjan, Lars Koekenbier, and Hermann Schulz-Baldes, Spectral localizer for line-gapped non-Hermitian systems, J. Math. Phys. (N.Y.) **64**, 082102 (2023).

[82] Jiho Noh, Wladimir A. Benalcazar, Sheng Huang, Matthew J. Collins, Kevin P. Chen, Taylor L. Hughes, and Mikael C. Rechtsman, Topological protection of photonic mid-gap defect modes, Nat. Photonics **12**, 408 (2018).

[83] Alexander Cerjan, Terry A. Loring, and Fredy Vides, Quadratic pseudospectrum for identifying localized states, J. Math. Phys. (N.Y.) **64**, 023501 (2023).

[84] Alexei Kitaev, Anyons in an exactly solved model and beyond, Ann. Phys. (Amsterdam) **321**, 2 (2006).

[85] Wenting Cheng, Alexander Cerjan, Ssu-Ying Chen, Emil Prodan, Terry A. Loring, and Camelia Prodan, Revealing topology in metals using experimental protocols inspired by K-theory, Nat. Commun. **14**, 3071 (2023).

[86] Benjamin J. Wieder and B. Andrei Bernevig, The axion insulator as a pump of fragile topology, arXiv:1810.02373.

[87] Christopher W. Peterson, Tianhe Li, Wladimir A. Benalcazar, Taylor L. Hughes, and Gaurav Bahl, A fractional corner anomaly reveals higher-order topology, Science **368**, 1114 (2020).

[88] Yuan Fang and Jennifer Cano, Filling anomaly for general two- and three-dimensional C_4 symmetric lattices, Phys. Rev. B **103**, 165109 (2021).